NANO LETTERS

Giant Terahertz Birefringence in an Ultrathin Anisotropic Semimetal

Edbert J. Sie,▶ Mohamed A. K. Othman,▶ Clara M. Nyby, Das Pemmaraju, Christina A. C. Garcia, Yaxian Wang, Burak Guzelturk, Chenyi Xia, Jun Xiao, Andrey Poletayev, Benjamin K. Ofori-Okai, Matthias C. Hoffmann, Suji Park, Xiaozhe Shen, Jie Yang, Renkai Li, Alexander H. Reid, Stephen Weathersby, Philipp Muscher, Nathan Finney, Daniel Rhodes, Luis Balicas, Emilio Nanni, James Hone, William Chueh, Thomas P. Devereaux, Prineha Narang, Tony F. Heinz, Xijie Wang, and Aaron M. Lindenberg*

Read Online

ACCESS | Metrics & More | Article Recommendations | Supporting Information

ABSTRACT: Manipulating the polarization of light at the nanoscale is key to the development of next-generation optoelectronic devices. This is typically done via waveplates using optically anisotropic crystals, with thicknesses on the order of the wavelength. Here, using a novel ultrafast electron-beam-based technique sensitive to transient near fields at THz frequencies, we observe a giant anisotropy in the linear optical response in the semimetal WTe$_2$ and demonstrate that one can tune the THz polarization using a 50 nm thick film, acting as a broadband wave plate with thickness 3 orders of magnitude smaller than the wavelength. The observed circular deflections of the electron beam are consistent with simulations tracking the trajectory of the electron beam in the near field of the THz pulse. This finding offers a promising approach to enable atomically thin THz polarization control using anisotropic semimetals and defines new approaches for characterizing THz near-field optical response at far-subwavelength length scales.

KEYWORDS: *terahertz, two-dimensional materials, tungsten ditelluride, waveplate, ultrafast electron diffraction*
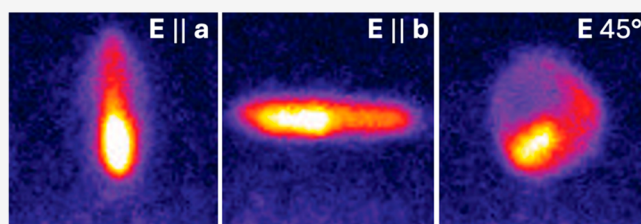
Birefringence is the optical property of a material in which the refractive index depends on the polarization of the incident light. It serves as a direct measure of broken symmetry and anisotropy in the structure of materials and acts as a probe of the novel electronic properties of materials, while simultaneously enabling numerous optoelectronic applications.[1,2] Birefringent materials are used to alter the polarization of light, either by rotating the angle of polarization or, as in the case of the quarter-wave plate, converting linearly polarized light into circularly polarized light. Typically, a thickness on the order of the incident wavelength is required to accumulate this phase shift in the birefringent material. For instance, quartz has a birefringence $\Delta n = 0.009$ at wavelength $\lambda = 590$ nm, where Δn is the difference in the index of refraction along the principal axes of the material. It becomes a quarter-wave plate with thickness $d = \lambda/(4\Delta n) = 16.4\,\mu m$. At a longer wavelength, $\lambda = 100\,\mu m$ ($\Delta n = 0.044$), it requires a significantly larger thickness of $d = 0.6$ mm to act as a quarter-wave plate. Here, we observed significant changes in the polarization state of a THz pulse, akin to quarter-wave plate behavior, using a WTe$_2$ crystal only 50 nm thick (thickness $\lambda/2000$). Prior studies have investigated other anisotropic van der Waals semiconductors such as black phosphorus, ReS$_2$, and ReSe$_2$, with thickness $\sim\lambda$,[3,4] quasi-1D semiconductor BaTiS$_3$ ($\sim\lambda/3$),[5] as well as the in-plane hyperbolic α-MoO$_3$ semiconductor,[6,7] all of which show smaller

birefringent responses. Recent efforts have additionally demonstrated novel types of polarization control at optical-near-IR wavelengths using atomically thin van der Waals materials but typically require cavity geometries to enhance the response in this ultrathin limit.[8,9] The characterization of the photonic properties of these materials in both the near and far field remains poorly developed, especially in the small sample, subwavelength limit.

WTe$_2$ is a layered semimetal with a strongly anisotropic in-plane structure.[10−13] The tungsten atoms dimerize along the crystallographic *a* axis and form an array of quasi-1D metallic chains. Despite having a structural resemblance to a wire-grid polarizer, the actual optical functionality of WTe$_2$ is more complex. To study the electrodynamic anisotropy of WTe$_2$, we used quasi-single-cycle broadband THz light pulses with a peak field of $\sim$625 kV/cm and a frequency centered at 3 THz sent at normal incidence through a 50 nm thick WTe$_2$ exfoliated crystal.
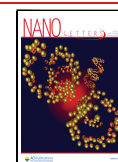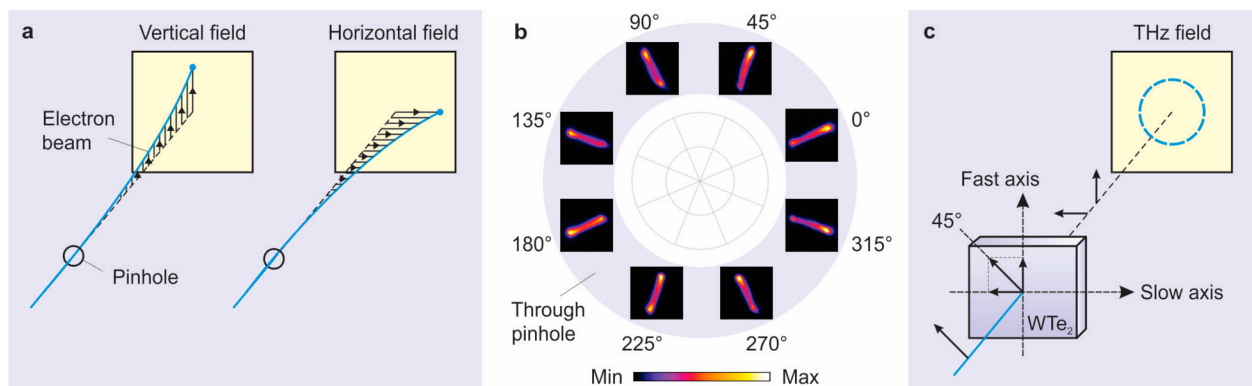
Figure 1. Streaking electrons using electric field from THz light pulses. (a) Electron beam is deflected along the vertical or horizontal direction depending on the electric field polarization. (b) Measured THz streaking of electron beams through a pinhole using THz light pulses at various linear polarization. (c) Schematic of circular streaking of electrons within a WTe$_2$ 50 nm thin film for a circularly polarized THz pulse in the near field.

Conventional means of characterizing THz polarization via electro-optic sampling or polarized detection of the transmitted light cannot be implemented straightforwardly because of the small lateral size of the sample (110 μm × 30 μm) relative to the THz spot size (~1 mm). In our experiments, the deflection of 100 fs relativistic electron bunches is measured to directly probe the THz polarization state in the near field.[14−16] This technique can discriminate the THz fields within the sample boundary by selectively probing the diffracted electron beam, even when the incident electron beam and terahertz spot sizes are significantly larger than those of the sample, thus providing sensitivity to the localized fields within a transversely small sample. The electrons have a relativistic kinetic energy of 3.1 MeV, which is crucial to ensure that the electron bunches travel at nearly the same speed (0.99c) as the THz light pulses, thus enabling measurement of the electric field polarization within the optical cycle of the THz light field. In particular, the electron bunches exhibit a momentum kick along the THz electric field polarization, referred to as THz streaking,[17−19] thus enabling direct mapping of the THz polarization via measurement of the electron trajectory.

Figure 1a illustrates the trajectory of the electron beam through a pinhole that exhibits THz streaking along the vertical or horizontal electric field direction. The electron beam is detected by a camera located downstream, from which the transverse displacement is measured. Figure 1b shows the experimentally measured streaking at various incident THz polarizations through a pinhole (without the WTe$_2$ sample). The finite pulse duration of the electron bunches and ~100 fs timing jitter resulted in an elongated streaking image, instead of a displaced point-like image, and show the as-expected linear trajectory along the incident THz polarization. This is in contrast to an otherwise undisturbed point-like image in the absence of an applied THz field. Such a fundamental, coherent light−matter interaction should occur not only for linear THz polarization but also for elliptical and circular THz polarizations (Figure 1c). The effect of THz streaking through WTe$_2$, with the crystallographic axes shown in Figure 2a,b, is well captured by the electron diffraction pattern from the sample (Figure 2c−f). In the absence of external fields, the diffraction pattern consisted of a two-dimensional array of point-like Bragg peaks along the crystallographic a and b axes (Figure 2c). In the presence of THz fields aligned along these axes, however, all of the Bragg peaks exhibited linear THz streaking, similar to the pinhole case, while preserving the diffraction pattern (Figure 2d,e). In particular, the
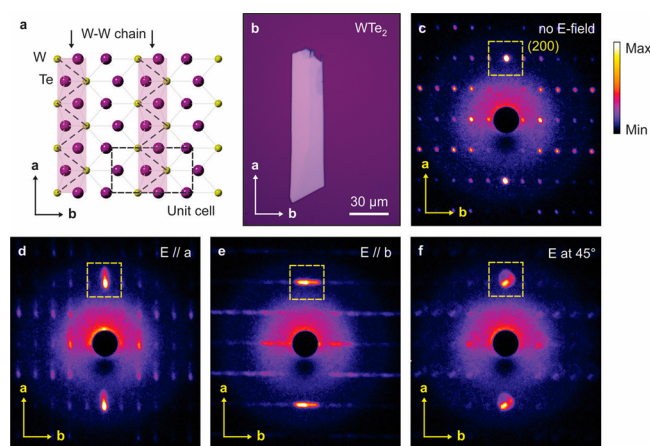

Figure 2. THz streaking nested in WTe$_2$ diffraction pattern. (a) Lattice structure of WTe$_2$ ab plane. (b) Optical microscope image of an exfoliated 50 nm thick, 110 μm × 30 μm WTe$_2$ sample on a SiO$_2$/Si substrate. (c) Measured electron diffraction pattern through WTe$_2$ with no applied THz E-field. (d−f) Measured electron diffraction pattern with THz E-field polarized along the a axis (d), along the b axis (e), and at 45° with respect to a and b axes (f).

electron beam deflected along the vertical and horizontal directions when the incident THz polarization is along the crystallographic a and b axes, respectively. Remarkably, when the THz field is polarized at 45° with respect to the a and b axes— thus sampling the anisotropic index of refraction—every Bragg peak showed a circular trajectory (Figure 2f), in stark contrast with the linear trajectory expected for isotropic materials (see Supplementary Movies M1−M4, showing that all Bragg peaks made this circular motion in a concerted manner only for the case where the THz field samples both a and b axes).

To investigate this unique streaking behavior, we isolated the brightest Bragg peak (200) and monitored the streaking image for various orientations of the linearly polarized incident THz field with respect to the b axis (Figure 3a). The streaking images show a clear progression from linear to elliptical to circular trajectories and then back to linear as we rotated the incident THz polarization through 90°. This behavior is identical with that of a quarter-wave plate. Note that the brightest intensity persisted at the center of every image, indicating the fraction of electron bunch (temporal duration ~100 fs) that trailed behind the THz pulse duration (~150 fs for the main cycle), also influenced by the timing jitter between electron and THz pulses.
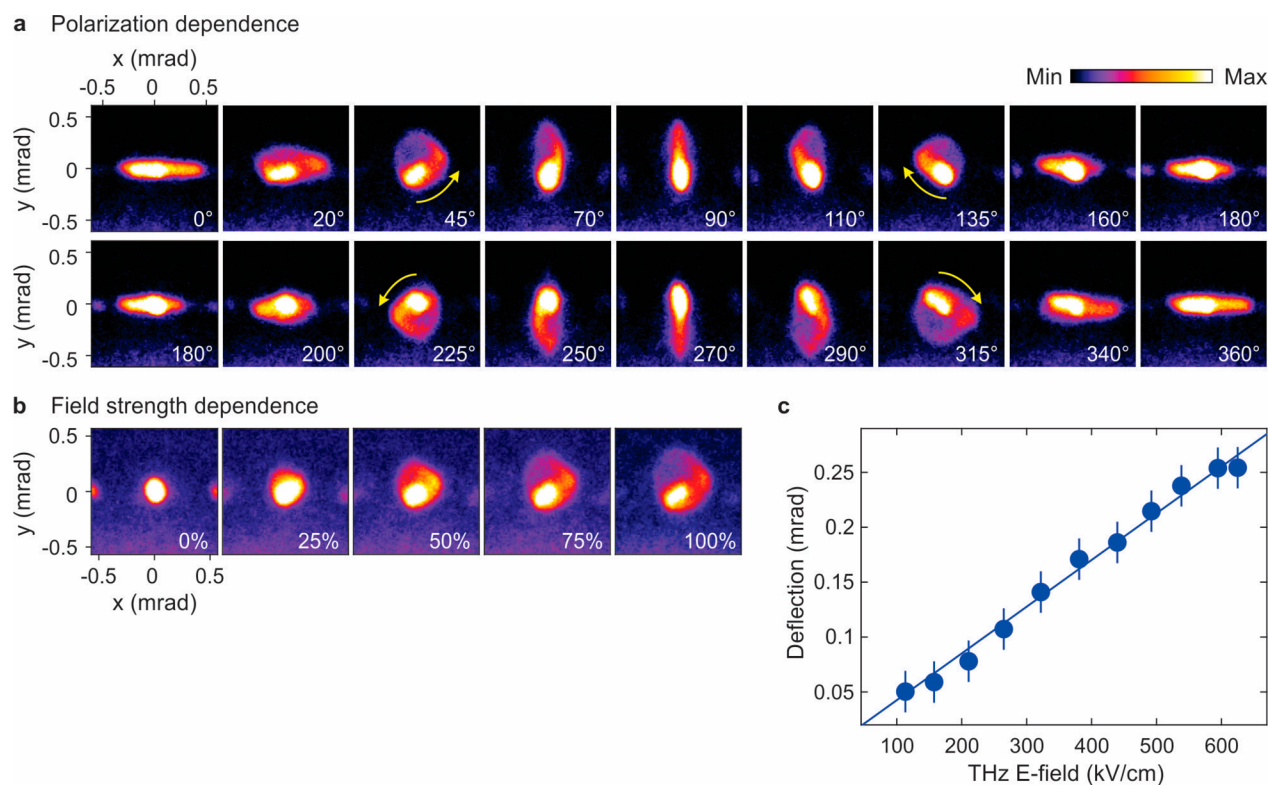
Figure 3. Polarization and field strength dependences of THz streaking. (a) Measured THz streaking at various incident THz polarizations through WTe$_2$. We obtained left-handed trajectories at 45 and 225° and right-handed trajectories at 135 and 315°. (b) Measured electron streaking trajectory (45°) at increasing THz electric field strength up to a maximum of 625 kV/cm. (c) Measured electron deflection amplitude at increasing THz electric field strength showing a linear dependence. The vertical error bars represent standard deviations.

We also found that the streaking diameter increased linearly with THz field at +45°, while preserving a circular trajectory (Figure 3b,c). This behavior is consistent with a deflection by the Lorentz force $\vec{F} = -e(\vec{E} + \vec{v} \times \vec{B})$ where both the electric and magnetic components of the THz field contribute linearly to the deflection, with opposite sign (see also Supporting Text S1).[15] Conversely, by tracking the electron deflection downstream we deduce the corresponding amplitude and polarization vector of the THz field in a time-resolved manner through the relation $\vec{E}(t) = E_0(\hat{x}\theta_x(t) + \hat{y}\theta_y(t))$, where E_0 (~0.8 MV/cm) is a proportionality constant and $\theta_x(t)$, $\theta_y(t)$ are the time-dependent deflections in milliradians. The linear increase of the deflection with the THz field (Figure 3c) further indicates that the birefringence we observed is a linear optical effect, which is independent of the incident electric field strength. Our observation is consistent with a recent measurement where circularly polarized THz light was prepared in advance and directly sent through a pinhole to deflect a copropagating electron beam.[20]

To determine the handedness of the circular polarization, we studied the electron trajectories through measurement of the streaking snapshots (+45°) at increasing time delay t between the electron bunch and the THz pulse (Figure 4a). Note that the snapshots are flipped images of the actual trajectories as seen from the electron beam source due to a folding mirror (after the phosphor screen) downstream to project an image onto the camera. In addition, the electron's deflection is opposite to the applied THz electric field due to the electron's negative charge in the Lorentz force (Supporting Text S1). Hence, the snapshots in Figure 4a provide an identical representation of the amplitude

and polarization vector of the THz electric field (in the near field). The trajectory started at the center of the image and rotated counterclockwise, with the loop spanning the upper half of the image. This behavior is consistent with a quasi-single cycle left-circularly polarized THz pulse, with the convention of handedness viewed from the light source. In this way we can assign the handedness of the other THz polarizations depicted in Figure 3a. That is, we obtained a left-circularly polarized THz pulse using an incident THz field polarized at +45 and +225° and a right-circularly polarized THz pulse using an incident field polarized at +135 and +315°. This is exactly the condition required to produce circularly polarized light by means of a quarter-wave plate. One can obtain the effective birefringence between the a and b axes through its phase retardation, $\Delta\phi = \frac{2\pi}{\lambda} d\Delta n$ where d is the sample thickness, Δn the effective birefringence, and λ the wavelength. By taking $d = 50$ nm and $\lambda = 100$ μm (3 THz) to produce an ideal quarter-wave phase retardation ($\Delta\phi = \pi/2$), we obtained an effective birefringence of $\Delta n = 500$. We note that the response is broadband with no indication of significant stretching of the incident field, as shown in Supporting Figure S6.

WTe$_2$ is a semimetal and it has a large dielectric function at THz frequencies similar to those in typical metals, e.g. aluminum and gold ($\varepsilon \approx 10^5$).[21,22] However, unlike most metals, WTe$_2$ is strongly anisotropic because of the spontaneous formation of quasi-1D metallic chains along the a axis[10] (Figure 2a). Although in principle the dielectric function has contributions from both electrons and phonons, our *ab initio* electronic structure calculations (DFT and diagrammatic techniques) and prior experiments showed that the intraband electronic
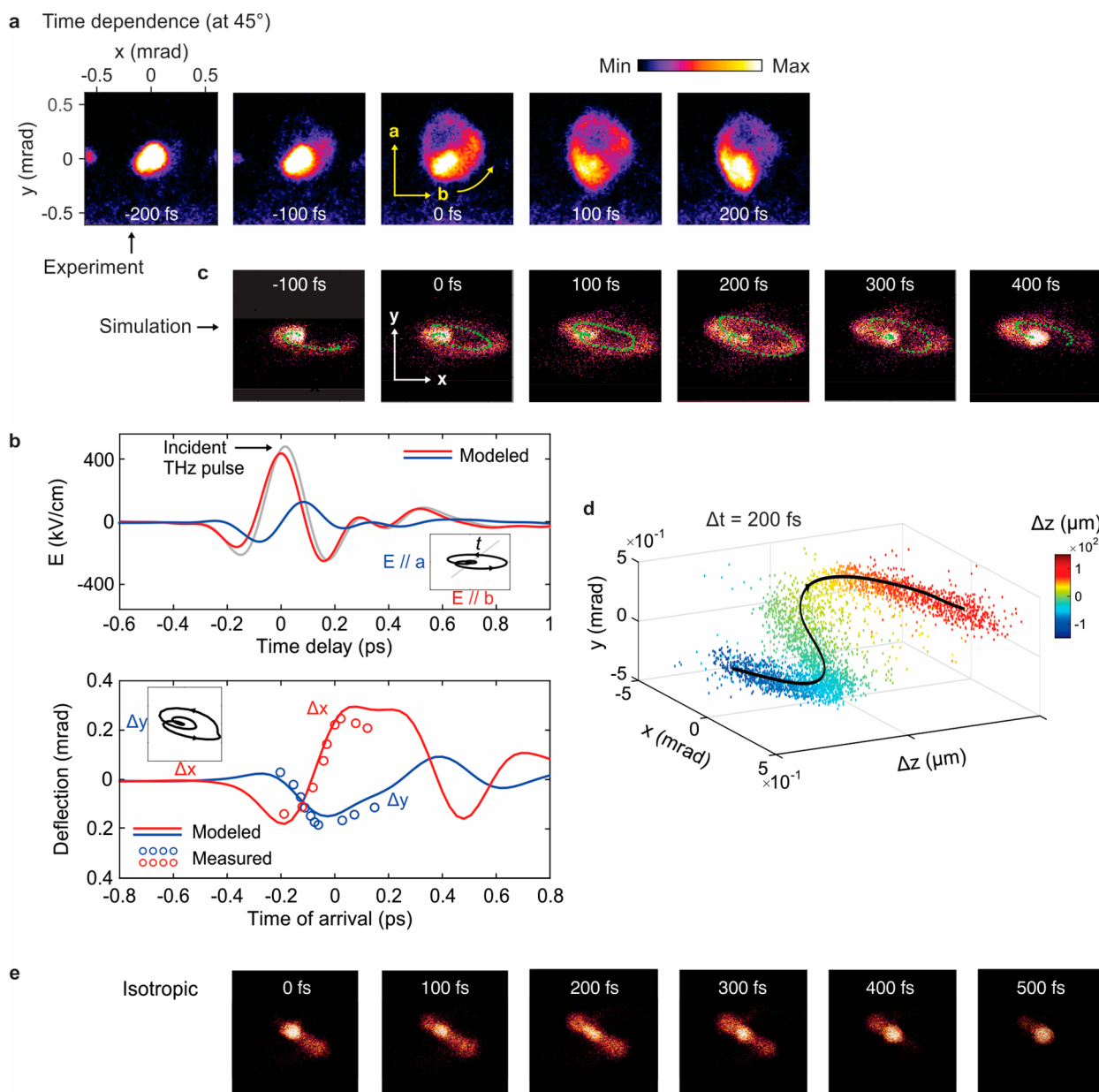
Figure 4. Capturing the THz trajectory motion in time. (a) Measured THz streaking at increasing time delay t between the electron bunch and the THz light pulse. The incident THz polarization is fixed at 45° with respect to the a and b axes. (b) (top panel) THz time profile measured using EO-sampling (gray), and simulated fields within the sample (at $z = 0$) decomposed along the in-plane a (vertical) and b (horizontal) axes, showing significant birefringence. (bottom panel) Simulated beam deflection at detector plane and decomposed into orthogonal components, as compared to data (extracted from measurements shown in (a)). (c) Modeled electron trajectory obtained from 3D simulations of the WTe$_2$ film interacting with the THz pulse in the near field, at $z = 0$, and at various time delays. (d) Simulated helical trajectory of electron in the near field. (e) Simulations comparing assumed isotropic to anisotropic optical properties.

contribution dominates the conductivity at THz frequencies (Supporting Text S4). Hence, the dielectric functions can be approximated using a Drude model.[23−25] In this model, the dielectric function is given by $\varepsilon \approx -\omega_{p,a,b}^2/(\omega^2 + i\omega/\tau_{a,b})$, which can be separated into real and imaginary parts, $\varepsilon_1 = -\omega_{p,a,b}^2/(\omega^2 + 1/\tau_{a,b}^2)$ and $\varepsilon_2 = (\omega_{p,a,b}^2/\omega\tau_{a,b})/(\omega^2 + 1/\tau_{a,b}^2)$, where the subscripts a and b define anisotropic values for the plasma frequency and scattering time along the two in-plane crystallographic axes. The distinct Drude behavior along the two axes is apparent from the anisotropy in the electronic band structure, i.e. strongly

dispersive along k_a and weakly dispersive along k_b,[11] with differing dc/ac conductivities. The real parts of the dielectric functions become very large and negative when approaching 3 THz and show significantly different values for light polarized along a and b axes,[23] consistent with the large and broadband birefringence we observed. Supporting Text S6 provides additional details on the Drude response of the film and estimates the required anisotropic materials parameters required to induce the observed large birefringences within an approximate 2D model for the transmitted field.[26] We find significant phase shifts approaching $\pi/3$ even within this simple model using values $\tau_a = 100$ fs, $\tau_b = 30$ fs, $\omega_{p,a} = 5800$ cm^{-1}, and $\omega_{p,b} = 4000$ cm^{-1}, with the anisotropic plasma frequencies

consistent with ref 23. Figure S9 shows the associated frequency dependent dielectric function in a Drude model using these values. Supporting Text S8 describes ab initio electronic structure calculations of the anisotropies in the scattering times and other Drude parameters. The *ab initio* calculation provides supporting evidence for significant anisotropies of the correct sign in the dielectric constant and in the induced phase shift but predicts somewhat smaller magnitudes in the anisotropic scattering times than experimentally extracted. We note that similar anisotropies in both the scattering times and Drude weights have been recently experimentally reported.[27] A quantitative model likely requires consideration of contributions beyond the simple Drude model.

To simulate and quantify more accurately the trajectories of the streaked electrons within the THz near field, we used a frequency domain finite-element solver to obtain both the electric and magnetic field 3D distribution and Fourier coefficients that represent the interaction of the THz pulse (with spectral content 0.1−5 THz) with the WTe_2 thin film, including the effects from the SiN window substrate, and by using the Drude model parameters given above. We used 30 Fourier coefficients to fully construct the frequency spectrum of the THz pulse. Snapshots of the electric fields in the $z−x$ plane in the vicinity of the sample show transient behavior of the field components and lead to a delay, or phase offset, between the two polarizations, shown in Figure 4b (more details are given in Supporting Text S10). Such 3D transient field maps were then used in space-charge particle tracking code (GPT*) to track the electrons from the UED rf-gun through the sample, downstream to the detector, following previous work.[19] The results, shown in Figure 4c, indicate that the electron trajectories track the polarization of the THz pulse in the near fields of the WTe_2 sample and show results consistent with experiment (Figure 4a). Figure 4d shows the simulated helical trajectory of the electron beam in the near field of the sample for the THz field incident at 45°. This behavior is obtained solely from material anisotropy when excited with polarization state at 45° with respect to the in-plane axes. Indeed, a film with isotropic properties only shows linear streaking (Figure 4e), proving that the material anisotropy plays a key role in the THz transmission and the near field response. Additionally, similar calculations in the large transverse film limit show that these effects are not arising solely from edge effects, which play a small role in the near field birefringence (Supporting Text S10).

The semimetal nature of this material renders the absorption coefficient larger than those found in typical birefringent materials but still corresponds to a rather high transmission coefficient in this nanoscale limit. We estimated using the best fit dielectric constant values from the experiment and in a 2d model for the complex transmission coefficient (eq S3) values of order 20% for the THz field for a 50 nm film. So while somewhat lossy, this shows a reasonably high transparency for nanoscale film thicknesses. Additional measurements described in Supporting Text S7 show tabletop THz transmission measurements with thicker WTe_2 samples and compare them to other isotropic systems, supporting these estimates.

In conclusion, we observed giant birefringence in anisotropic semimetal WTe_2 by characterizing the THz polarization state in the near field through the deflection of femtosecond diffracted electrons. Such a large birefringence arises from the strongly anisotropic structure of WTe_2 as the metallic W ions dimerize along the crystalline *a* axis and form an array of quasi-1D metallic chains. Our finding suggests the use of WTe_2 for potential applications with respect to THz circular dichroism and characterization of chiral materials.[28] For instance, the recently observed spontaneous gyrotropic electronic order in 1T-TiSe$_2$ allows one to induce chirality on demand using circularly polarized far-infrared light in the near field,[29] and this should extend to a broader class of materials with energy gaps at THz frequencies. Our findings furthermore provide a new means for characterizing electromagnetic fields in the near field of materials, including possible hyperbolic responses.[27,30] More broadly, this work demonstrates new possibilities for the development of ultrathin waveplates for on-chip two-dimensional optoelectronic applications at THz frequencies.[31−35]

■ ASSOCIATED CONTENT

Data Availability Statement

The data that support the findings of this study are available from the corresponding author on reasonable request.

Ⓢ Supporting Information

The Supporting Information is available free of charge at https://pubs.acs.org/doi/10.1021/acs.nanolett.4c00758.

> Materials and methods, THz-streaking of electron beam, sample dielectric environment and orientation with respect to Si frame edge, DFT calculations on phonons and interband optical excitations, broadband nature of response, birefringent response of transmitted field, additional evidence of WTe_2 birefringence from a tabletop THz transmission, electronic structure theory calculations on intraband transitions (Drude lifetimes, conductivity, and dielectric functions), direct sampling using diffracted electron bean in UED, and modeling of transient streaking dynamics through interaction with a birefringent film (PDF)

> THz streaking through a pinhole at increasing time delay (MOV)

> THz streaking through 50 nm thick WTe_2 with field polarized along *a* axis (MOV)

> THz streaking through 50 nm thick WTe_2 with field polarized along *b* axis (MOV)

> THz streaking through 50 nm thick WTe_2 with field polarized at 45° from *a* axis (MOV)

■ AUTHOR INFORMATION

Corresponding Author

Aaron M. Lindenberg − *Stanford Institute for Materials and Energy Sciences (SIMES) and Stanford PULSE Institute, SLAC National Accelerator Laboratory, Menlo Park, California 94025, United States; Department of Materials Science and Engineering, Stanford University, Stanford, California 94305, United States;* Ⓞ orcid.org/0000-0003-3233-7161; Email: aaronl@stanford.edu

Authors

Edbert J. Sie − *Geballe Laboratory for Advanced Materials, Stanford University, Stanford, California 94305, United States; Stanford Institute for Materials and Energy Sciences (SIMES), SLAC National Accelerator Laboratory, Menlo Park, California 94025, United States*

Mohamed A. K. Othman − *SLAC National Accelerator Laboratory, Menlo Park, California 94025, United States*

Clara M. Nyby − *Department of Chemistry, Stanford University, Stanford, California 94305, United States*

Das Pemmaraju — *Stanford Institute for Materials and Energy Sciences (SIMES), SLAC National Accelerator Laboratory, Menlo Park, California 94025, United States*

Christina A. C. Garcia — *John A. Paulson School of Engineering and Applied Sciences, Harvard University, Cambridge, Massachusetts 02138, United States*

Yaxian Wang — *John A. Paulson School of Engineering and Applied Sciences, Harvard University, Cambridge, Massachusetts 02138, United States;* orcid.org/0000-0003-4790-2880

Burak Guzelturk — *X-ray Science Division, Advanced Photon Source, Argonne National Laboratory, Lemont, Illinois 60439, United States;* orcid.org/0000-0003-1977-6485

Chenyi Xia — *Department of Materials Science and Engineering, Stanford University, Stanford, California 94305, United States*

Jun Xiao — *Department of Materials Science and Engineering, Stanford University, Stanford, California 94305, United States; Department of Materials Science and Engineering, University of Wisconsin-Madison, Madison, Wisconsin 53706, United States;* orcid.org/0000-0003-4248-8190

Andrey Poletayev — *Department of Materials Science and Engineering, Stanford University, Stanford, California 94305, United States;* orcid.org/0000-0002-7892-8963

Benjamin K. Ofori-Okai — *SLAC National Accelerator Laboratory, Menlo Park, California 94025, United States*

Matthias C. Hoffmann — *SLAC National Accelerator Laboratory, Menlo Park, California 94025, United States*

Suji Park — *Stanford Institute for Materials and Energy Sciences (SIMES), SLAC National Accelerator Laboratory, Menlo Park, California 94025, United States;* orcid.org/0000-0002-2269-7705

Xiaozhe Shen — *SLAC National Accelerator Laboratory, Menlo Park, California 94025, United States*

Jie Yang — *SLAC National Accelerator Laboratory, Menlo Park, California 94025, United States*

Renkai Li — *SLAC National Accelerator Laboratory, Menlo Park, California 94025, United States*

Alexander H. Reid — *SLAC National Accelerator Laboratory, Menlo Park, California 94025, United States;* orcid.org/0000-0002-7587-295X

Stephen Weathersby — *SLAC National Accelerator Laboratory, Menlo Park, California 94025, United States*

Philipp Muscher — *Stanford Institute for Materials and Energy Sciences (SIMES), SLAC National Accelerator Laboratory, Menlo Park, California 94025, United States*

Nathan Finney — *Department of Mechanical Engineering, Columbia University, New York, New York 10027, United States*

Daniel Rhodes — *Department of Mechanical Engineering, Columbia University, New York, New York 10027, United States;* orcid.org/0000-0002-7651-3211

Luis Balicas — *National High Magnetic Field Laboratory and Department of Physics, Florida State University, Tallahassee, Florida 32310, United States;* orcid.org/0000-0002-5209-0293

Emilio Nanni — *SLAC National Accelerator Laboratory, Menlo Park, California 94025, United States*

James Hone — *Department of Mechanical Engineering, Columbia University, New York, New York 10027, United States;* orcid.org/0000-0002-8084-3301

William Chueh — *Stanford Institute for Materials and Energy Sciences (SIMES), SLAC National Accelerator Laboratory, Menlo Park, California 94025, United States; Department of Materials Science and Engineering and Department of Applied Physics, Stanford University, Stanford, California 94305, United States;* orcid.org/0000-0002-7066-3470

Thomas P. Devereaux — *Stanford Institute for Materials and Energy Sciences (SIMES), SLAC National Accelerator Laboratory, Menlo Park, California 94025, United States; Department of Materials Science and Engineering, Stanford University, Stanford, California 94305, United States*

Prineha Narang — *College of Letters and Science, University of California, Los Angeles, California 90095, United States*

Tony F. Heinz — *Stanford Institute for Materials and Energy Sciences (SIMES) and Stanford PULSE Institute, SLAC National Accelerator Laboratory, Menlo Park, California 94025, United States; Department of Applied Physics, Stanford University, Stanford, California 94305, United States*

Xijie Wang — *SLAC National Accelerator Laboratory, Menlo Park, California 94025, United States; Faculty of Physics, University of Duisburg-Essen, 47057 Duisburg, Germany; Department of Physics, University of Dortmund, 44221 Dortmund, Germany*

Complete contact information is available at:
https://pubs.acs.org/10.1021/acs.nanolett.4c00758

Author Contributions

▶E.J.S. and M.A.K.O. contributed equally.

Notes

The authors declare no competing financial interest.

■ ACKNOWLEDGMENTS

■ REFERENCES

(1) Xia, F.; Wang, H.; Xiao, D.; Dubey, M.; Ramasubramaniam, A. Two-dimensional material nanophotonics. *Nat. Photonics* **2014**, *8*, 899−907.

(2) McIver, J. W.; Hsieh, D.; Steinberg, H.; Jarillo-Herrero, P.; Gedik, N. Control over topological insulator photocurrents with light polarization. *Nat. Nanotechnol.* **2012**, *7*, 96−100.

(3) Yang, H.; et al. Optical Waveplates Based on Birefringence of Anisotropic Two-Dimensional Layered Materials. *ACS Photonics* **2017**, *4*, 3023−3030.

(4) Mao, N.; et al. Optical Anisotropy of Black Phosphorus in the Visible Regime. *J. Am. Chem. Soc.* **2016**, *138*, 300−305.

(5) Niu, S.; et al. Giant optical anisotropy in a quasi-one-dimensional crystal. *Nat. Photonics* **2018**, *12*, 392−396.

(6) Ma, W.; et al. In-plane anisotropic and ultra-low-loss polaritons in a natural van der Waals crystal. *Nature* **2018**, *562*, 557−562.

(7) Folland, T. G.; Caldwell, J. D. Precise control of infrared polarization. *Nature* **2018**, *562*, 499−501.

(8) Biswas, S.; Grajower, M. Y.; Watanabe, K.; Taniguchi, T.; Atwater, H. A. Broadband electro-optic polarization conversion with atomically thin black phosphorus. *Science* **2021**, *374*, 448−453.

(9) Zhang, H.; et al. Cavity-enhanced linear dichroism in a van der Waals antiferromagnet. *Nat. Photonics* **2022**, *16*, 311−317.

(10) Mar, A.; Jobic, S.; Ibers, J. A. Metal-metal vs tellurium-tellurium bonding in WTe$_2$ and its ternary variants TaIrTe$_4$ and NbIrTe$_4$. *J. Am. Chem. Soc.* **1992**, *114*, 8963−8971.

(11) Ali, M. N.; et al. Large, non-saturating magnetoresistance in WTe$_2$. *Nature* **2014**, *514*, 205−208.

(12) Muscher, P. K.; et al. Highly Efficient Uniaxial In-Plane Stretching of a 2D Material via Ion Insertion. *Adv. Mater.* **2021**, *33*, 2101875.

(13) Sie, E. J.; et al. An ultrafast symmetry switch in a Weyl semimetal. *Nature* **2019**, *565*, 61−66.

(14) Ofori-Okai, B. K.; et al. A terahertz pump mega-electron-volt ultrafast electron diffraction probe apparatus at the SLAC Accelerator Structure Test Area facility. *J. Instrum.* **2018**, *13*, P06014−P06014.

(15) Li, R. K.; et al. Terahertz-based subfemtosecond metrology of relativistic electron beams. *Phys. Rev. Accel. Beams* **2019**, *22*, 012803.

(16) Baek, I. H.; et al. Real-time ultrafast oscilloscope with a relativistic electron bunch train. *Nat. Commun.* **2021**, *12*, 6851.

(17) Frühling, U. Light-field streaking for FELs. *J. Phys. B: At. Mol. Opt. Phys.* **2011**, *44*, 243001.

(18) Curry, E.; Fabbri, S.; Maxson, J.; Musumeci, P.; Gover, A. Meter-Scale Terahertz-Driven Acceleration of a Relativistic Beam. *Phys. Rev. Lett.* **2018**, *120*, 094801.

(19) Othman, M. A. K.; et al. Measurement of femtosecond dynamics of ultrafast electron beams through terahertz compression and time-stamping. *Appl. Phys. Lett.* **2023**, *122*, 141107.

(20) Zhao, L.; et al. Terahertz Oscilloscope for Recording Time Information of Ultrashort Electron Beams. *Phys. Rev. Lett.* **2019**, *122*, 144801.

(21) Rakić, A. D.; Djurišić, A. B.; Elazar, J. M.; Majewski, M. L. Optical properties of metallic films for vertical-cavity optoelectronic devices. *Appl. Opt.* **1998**, *37*, 5271.

(22) Ordal, M. A.; et al. Optical properties of the metals Al, Co, Cu, Au, Fe, Pb, Ni, Pd, Pt, Ag, Ti, and W in the infrared and far infrared. *Appl. Opt.* **1983**, *22*, 1099.

(23) Frenzel, A. J.; et al. Anisotropic electrodynamics of type-II Weyl semimetal candidate WTe$_2$. *Phys. Rev. B* **2017**, *95*, 245140.

(24) Kimura, S.-i.; et al. Optical evidence of the type-II Weyl semimetals ${\mathrm{MoTe}}_{2}$ and ${\mathrm{WTe}}_{2}$. *Phys. Rev. B* **2019**, *99*, 195203.

(25) Homes, C. C.; Ali, M. N.; Cava, R. J. Optical properties of the perfectly compensated semimetal WTe$_2$. *Phys. Rev. B* **2015**, *92*, 161109.

(26) Li, Y.; Heinz, T. F. Two-dimensional models for the optical response of thin films. *2D Materials* **2018**, *5*, 025021.

(27) Wang, C.; et al. Van der Waals thin films of WTe$_2$ for natural hyperbolic plasmonic surfaces. *Nat. Commun.* **2020**, *11*, 1158.

(28) Narang, P.; Garcia, C. A. C.; Felser, C. The topology of electronic band structures. *Nat. Mater.* **2021**, *20*, 293.

(29) Xu, S. Y.; et al. Spontaneous gyrotropic electronic order in a transition-metal dichalcogenide. *Nature* **2020**, *578*, 545−549.

(30) Wang, H.; Low, T. Hyperbolicity in two-dimensional transition metal ditellurides induced by electronic bands nesting. *Phys. Rev. B* **2020**, *102*, 241104.

(31) Gao, L.; et al. On-chip plasmonic waveguide optical waveplate. *Sci. Rep.* **2015**, *5*, 15794.

(32) Nouman, M. T.; Hwang, J. H.; Jang, J. H. Ultrathin Terahertz Quarter-wave plate based on Split Ring Resonator and Wire Grating hybrid Metasurface. *Sci. Rep.* **2016**, *6*, 39062.

(33) Zhao, Y.; Alù, A. Manipulating light polarization with ultrathin plasmonic metasurfaces. *Phys. Rev. B* **2011**, *84*, 205428.

(34) Yu, S.; Wu, X.; Wang, Y.; Guo, X.; Tong, L. 2D Materials for Optical Modulation: Challenges and Opportunities. *Adv. Mater.* **2017**, *29*, 1606128.

(35) Low, T.; et al. Polaritons in layered two-dimensional materials. *Nat. Mater.* **2017**, *16*, 182−194.